Static Instability Analysis of Long-Span Cable-Stayed Bridges with Carbon Fiber Composite Cable under Wind Load

Chin-Sheng Kao[1]*, Chang-Huan Kou[2] and Xu Xie[3]

[1]*Department of Construction, Tamkang University, Tamsui, Taiwan 251, R.O.C.*
[2]*Department of Civil Engineering, Chunghua University, Hsinchu, Taiwan 300, R.O.C.*
[3]*Department of Civil Engineering, Zhejiang University, Zhejiang, China*

Abstract

In this paper, a three dimensional analysis is performed to investigate the static instability of long-span cable-stayed bridges due to wind loading. Cables made of carbon fiber composite cable (CFCC) are studied. Nonlinearity due to displacement-dependent wind loading is considered. A 1400-meter cable-stayed bridge model is used to investigate the static behavior of bridges with both steel and CCFC cable. The static instability of the bridges, both after completion as well as under construction, is considered. This study concludes that the static stability of CFCC long-span cable-stayed bridges simulates that of steel cable-stayed bridges. It is also shown that the instability phenomenon occurs when the wind attack angle acting on the girder exceeds 5 degrees.

Key Words: Cable-stayed Bridge, Static Instability, Carbon Fiber Composite Cable

1. Introduction

Remarkable increases in the span length of cable-stayed bridges have been achieved over the past few years. For example, the Sutong Bridge, with a span of 1088 meters, is currently under construction in China. To prevent degradation of the cables in these bridges from fatigue and corrosion, use of carbon fiber composite cable (CFCC) has been considered [1–3]. The behavior of long-span cable-stayed bridges using CFCC is addressed in this paper.

Kao [4] examined the ultimate strength of long-span cable-stayed bridges with CFCC. He compared the behavior of both steel cable (SC) and CFCC using a 3 dimensional elasto-plastic large displacement analysis. It was shown that the ultimate strength of the bridge using CFCC was greater than the bridge using SC because CFCC retained axial stiffness until the collapse load of the girder was reached. In addition, the compressive stress in cross-sections of both the girder and the tower does not increase under design load intensity because the weight of CFCC is significantly below that of steel.

To ensure safety, however, against out-of-plane static instability in the design of long-span cable-stayed bridges is an important issues, because the flutter onset wind velocity of long-span cable-stayed bridges is larger than static instability one [5], and also the width of the girder is controlled by this instability problem.

In this paper, a 3-D geometrically nonlinear finite element model [4] of a 1400-meter cable-stayed bridge is used to analyze the static instabilities of the bridge. Wind loadings, both during and after completion of construction, are considered. Comparison of the behavior of this long-span cable-stayed bridge using both CFCC and SC is presented. Displacement-dependent [6] wind loading acting on the girder, cables, and towers is employed. Here,

*Corresponding author. E-mail: csk@mail.tku.edu.tw

aerodynamic coefficients are expressed as a function of the wind attack angle. Thus, when the girder displaces under three components of wind load, (i.e. lift force, drag force, and aerodynamic moment), the wind load actually varies because of the rotation of the girder and the variation of the horizontal projection of the girder.

2. Bridge Model

Figure 1 provides the details of the 1400 meter self-anchored cable-stayed bridge used in this study [6–8]. The deck accommodates 4 lanes of traffic. A side-view of the bridge and a front-view of the tower are given. The side span length is nearly half of the center span length and, in the side span, three intermediate piers are installed at a distance of 100 meters in order to increase in-plane flexural rigidity of the bridge. The height of the tower from the deck level is one fifth of the center span length. Cables, spaced at 20 meters, suspend the girder.

The cross-sectional shape of the girder is shown in Figure 1(b). The width (Bu) and the depth of the girder is assumed to be 30 meters and 4.6 meters respectively. A 12 mm thickness is assumed for both the deck and lower flange. The longitudinally arranged ribs (which are expected to bear the axial force) have an assumed thickness of 20 mm. Five inner ribs (of thickness 15 mm) are employed. The flexural rigidity of the girder near this tower is increased. This is accomplished by using the thicker plate shown in Figure 1 (b). The distance (Xu) of the above reinforcement, in the direction of the bridge axis, is 140 meters. The thickness of plate of the tower is 30 mm and equivalent thickness and the thickness of the longitudinally arranged ribs is 10 mm.

Preliminary design cross-sectional properties are listed in Table 1.

The design conditions used for the analysis of cable-stayed bridge of this paper (using SC) are provided in reference 7. The yield point of the steel plate is 4.511×10^5

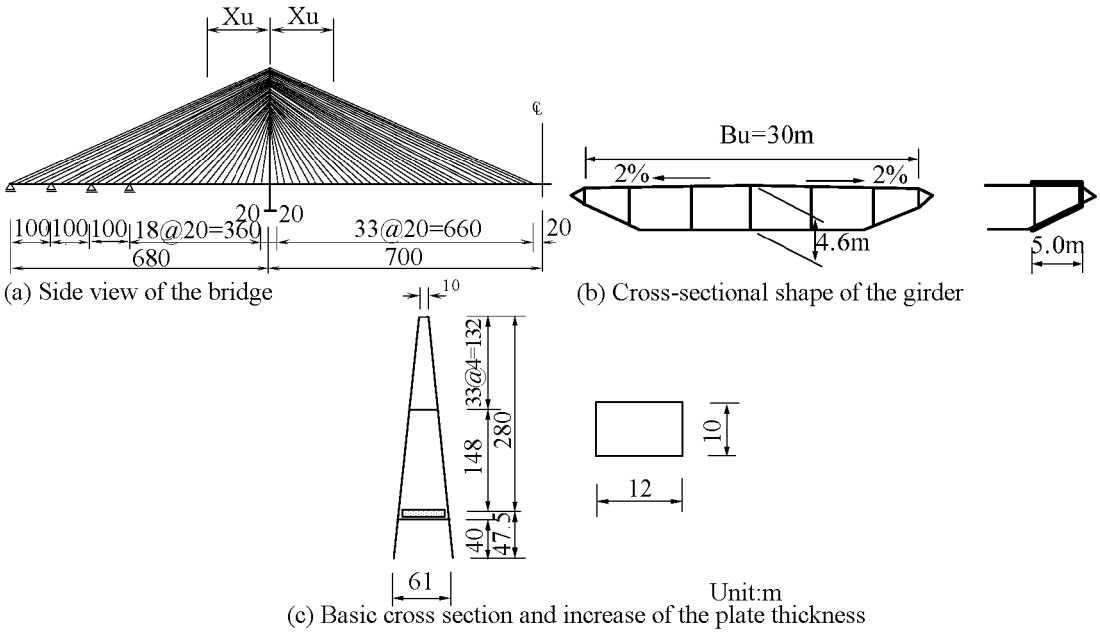

Figure 1. 1400-meter cable-stayed bridge model.

Table 1. Cross sectional properties (Unit: m, m^2 or m^4)

Member	Cross-sectional area	In-plane moment of inertia of area	Out-of-plane moment of inertia of area	St. Venante torsion constant*
Girder 1 (Basic)	1.647	5.759	131.575	11.145
Girder 2 (Reinforced)	2.299	7.182	240.355	14.489
Tower (per one column)	1.760	30.667	40.320	39.273

*neglecting longitudinal ribs.

kN/m^2 and Yong's modulus is 2.07×10^8 kN/m^2. The yield stress, breaking stress, modulus and allowable stress of both SC and CFCC are shown in Table 2.

Dead load per unit length (W_D) is calculated as

$$W_D = (1.4A_s) \times \gamma_s + 70.0 \quad (1)$$

Where, A_s is the cross-sectional area of the girder which bears axial force. The coefficient of 1.4 is to take into account the load from diaphragms and cross frames, etc. γ_s is the weight density of steel (= 77 KN/m^3) and the value 70.0 (KN/m) is the superimposed dead load, such as the pavement, handrail and attachment, etc. The initial tension in cables under dead load is determined based on the condition that the bending moment in the tower is zero and that in the girder nearly zero. They are so determined that their vertical components correspond to reactions of a continuous beam. The beam is supported at points where the cables are anchored to the girder and is subjected to dead load. In this analysis, the condition for closure of the girder is taken into account when determining initial tension in the cables. Maximum tension of the cables caused by live load is assumed to be 25% of initial tension under dead load. Figure 2 shows the crosssectional area and sag of the cables.

3. Analysis under Displacement-dependent Wind Load

A 3D geometrical nonlinear analysis is employed [6–8]. For this model, a 4-node isoparametric cable element is used [9]. With this element, the wind load acting on the cable is taken into account. The change of the tension in cables as well as its change in direction is considered. The following three components of wind load are applied to the girder (see Figure 3).

$$\begin{cases} D(\alpha) = 0.5\rho U_z^2 A_n C_D(\alpha) \\ L(\alpha) = 0.5\rho U_z^2 B C_L(\alpha) \\ M(\alpha) = 0.5\rho U_z^2 B^2 C_M(\alpha) \end{cases} \quad (2)$$

where, D, L and M are the drag force, lift force and aerodynamic moment, respectively, ρ is the air density [10]. A_n and B are the horizontal projection and total width of the girder, respectively. C_D, C_L and C_M are aerodynamic coefficients and α is the wind attack angle.

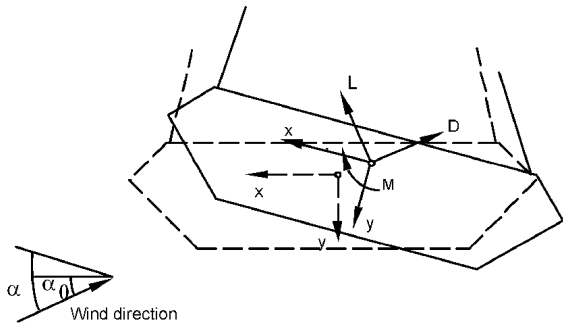

Figure 3. Wind load acting on the girder.

Table 2. Material properties of steel cable and carbon fiber composite cable (Unit: kN/m^2)

Type	Yield stress	Breaking stress	Young's modulus	Allowable stress
Steel cable	1.1564×10^6	1.568×10^6	1.96×10^8	6.0×10^5
CFCC [1]	2.450×10^6	2.450×10^6	1.65×10^8	8.17×10^5

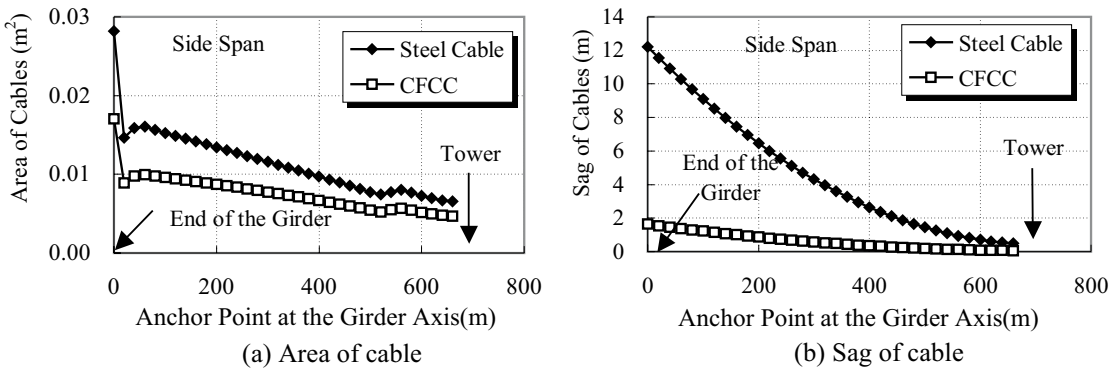

Figure 2. Area and sag of cables (1/4 bridge and one cable pane).

U_z is the wind velocity at the height of z, and is given by

$$U_Z = (\frac{Z}{10})^{\frac{1}{7}} U_{10} \tag{3}$$

Where, U_{10} is the wind velocity at the height of 10 meters.

Figure 4 shows the wind loading of the cable. In the figure, the wind load (D_c) per unit length is expressed as

$$D_C = N_1 D_{C1} + N_2 D_{C2} + N_3 D_{C3} + N_4 D_{C4} \tag{4}$$

where, Ni (i = 1~4) are the shape function of the cable and D_{ci} (i = 1~4) are the drag force at the height of node i, and are given by

$$D_{Ci} = 0.5 \rho U_{zi}^2 \phi C_{Dc} \tag{5}$$

Where, C_{Dc}, is the drag coefficient which is acting on the cable element, ϕ is the diameter of cable.

Figure 5 shows aerodynamic coefficients depending on the wind attack angle [11]. These values, which were obtained from wind tunnel testing, are for a long-span cable-stayed bridge. We cite this data because the dimensions of the streamlined cross sections used to obtain them are very similar to Figure (1b). Table 3 shows the dimension of each streamlined cross section. The dimensions of type I are nearly same the bridge model shown in Figure 1.

In this analysis, the drag coefficient of the tower and the cable are assumed to be 1.2 and 0.7 respectively.

4. Results and Discussion

Figure 6 shows the rotational angle of the bridge both

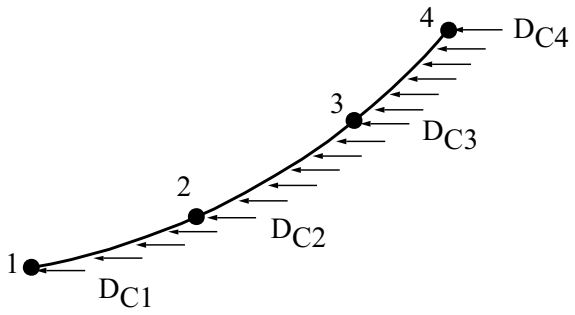

Figure 4. Wind load acting on cables.

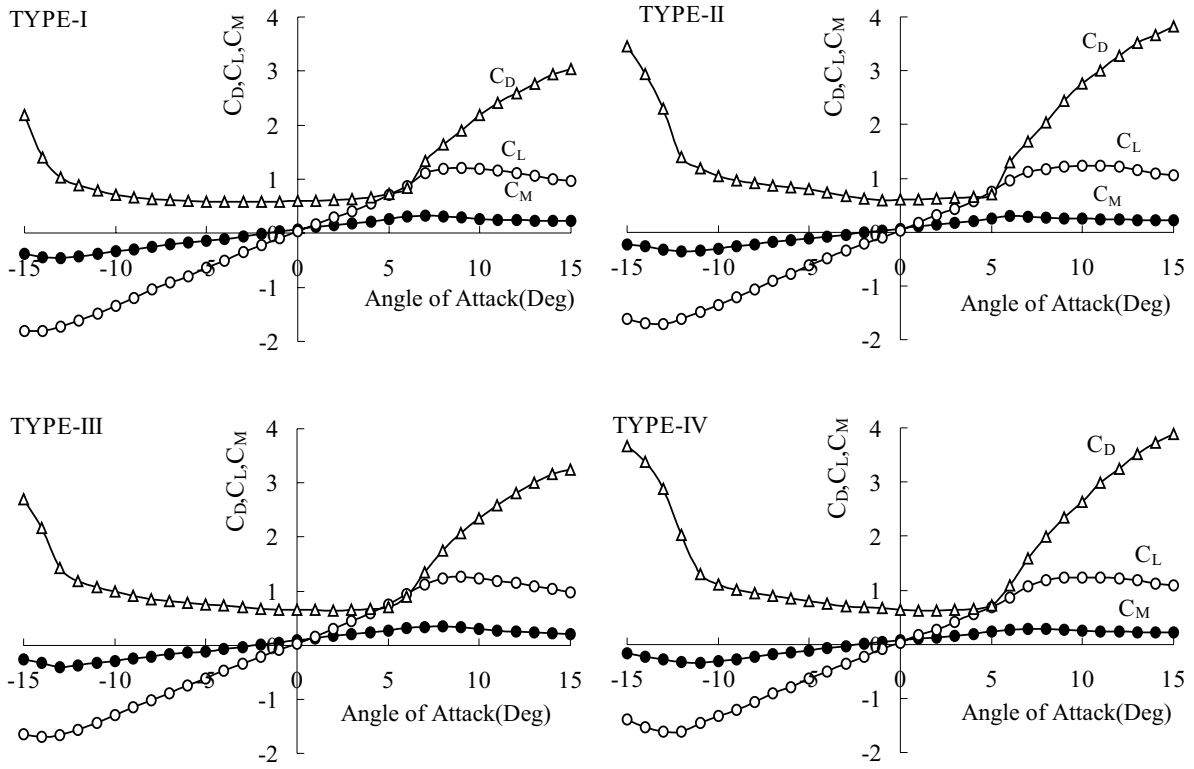

Figure 5. Aerodynamic coefficients.

Table 3. Prototype dimensions of streamlined cross section in wind tunnel test

Cross section	Width (Bu) (m)	Depth at center of the cross section (m)	Depth at end of the cross section (m)
TYPE-I	30	4.6	2.3
TYPE-II	36	4.0	2.0
TYPE-III	34	4.6	2.3
TYPE-IV	40	4.2	2.1

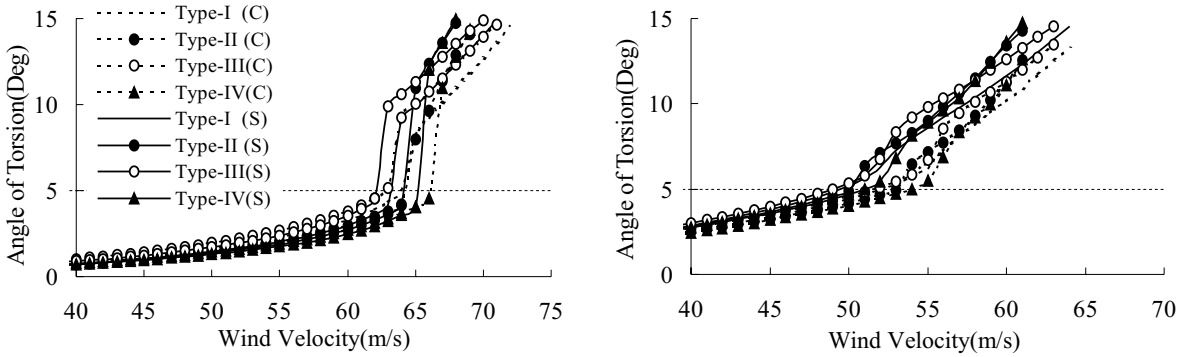

(a) After completion (b) Before closure of the girder

Figure 6. Torsion angle of the girder at center point of the span.

after completion as well as before closure of the girder. The cantilevered erection method has been employed. The rotational angle is measured at the center of the span. In the figure, the horizontal axis begins with a wind velocity of 40 m/s (i.e. wind velocities less than 40 m/s show no variation). From Figure 6, it is shown that the structure remains stable up to a rotational angle of 5 degrees. Note however that a slight difference of this angle is obtained depending on the cable material and the aerodynamic coefficients. When the wind velocity increases to about 62 m/s, the behavior of the rotational angle of the bridge after completion becomes unstable. A wind velocity of about 50 m/s produces instability in the bridge under construction.

Of significant importance is the jumping phenomenon that occurs when the wind attack angle approaches 5 degrees on the completed bridge. This phenomenon is observed regardless of the aerodynamic coefficients and material of the cable. The reason for this jump is related to the drag coefficient, C_D. Note that C_D increases rapidly at a 5 degree of wind attack angle as shown in Figure 5. A complete understanding of this phenomenon is very important, because unstable onset wind velocity is only about 62 m/s.

Figure 7 gives the horizontal displacement, at the center of the span, as a function of wind velocity. The results

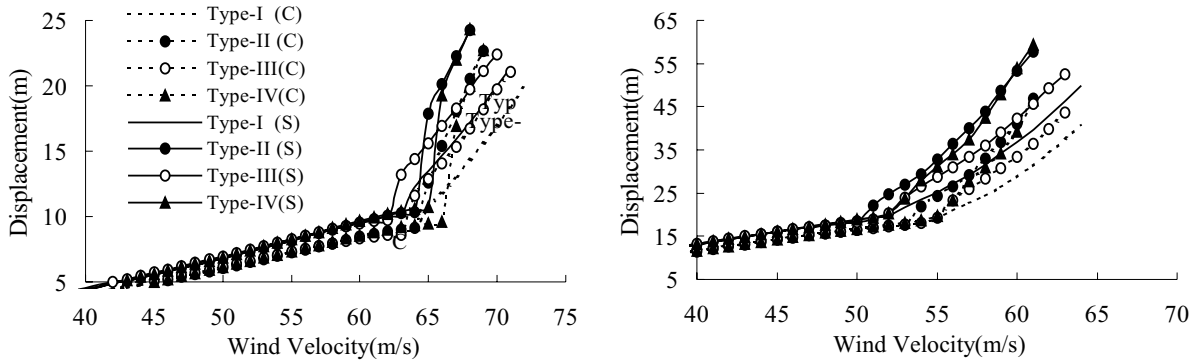

(a) After completion (b) Before closure of the girder

Figure 7. Horizontal displacement at center of the span.

of the bridge after completion and the bridge before closure of the girder are provided in Figure 7(a) and Figure 7(b) respectively. From these diagrams, it is seen that the response of horizontal displacement in the CFCC bridges is approximately 10% lower than that of the girder in the SC bridges. Thus, only modest differences in stability are influenced by the material of the cables.

Figure 8 shows the vertical deflection at the center of the girder in both brides both after completion and under construction. When the wind velocity reaches approximately 62 m/s, an instability phenomenon occurred in the completed bridge. Comparing with the behavior of torsional angle and horizontal displacement, nearly same behavior of vertical deflection is obtained.

From above results, a map tracking the girder cross-section under wind load can be made. Figure 9 shows this tracking map of the girder cross-section, at the center of the span, when CFCC is used. In this figure, the horizontal axis is the horizontal displacement and vertical axis is the vertical displacement. The three joined points are the left anchor point, center of the cross-section, and right anchor point. Each triplet shown is an increment of wind velocity of 2 m/s. From this figure, it is clearly shown that the jumping phenomenon occurs in the completed bridge at 64 m/s wind velocity. In the bridge under construction, a wind velocity of 54 m/sec is the onset of a more rapid displacement, but not a clearly defined jumping phenomenon.

In previous studies [8], they used smoothed aerodynamic coefficients to investigate the behavior of the same bridge model under wind load. Though the unstable behavior was obtained at the wind velocity of around 80 m/s, jumping phenomenon did not occur. This indicates that aerodynamic coefficients of the girder are very important in static instability analysis of long-span cable-stayed bridges.

5. Concluding Remarks

Using a 1400-meter cable-stayed bridge, the effect of

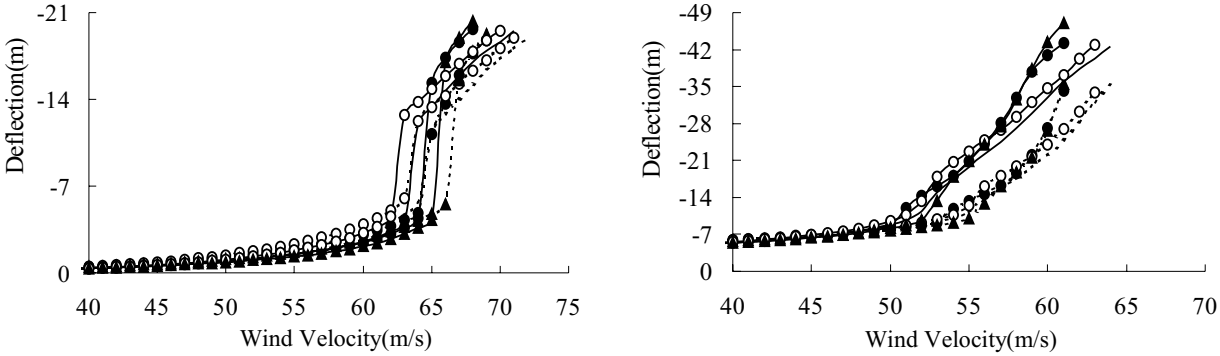

Figure 8. Vertical deflection at center of the span.

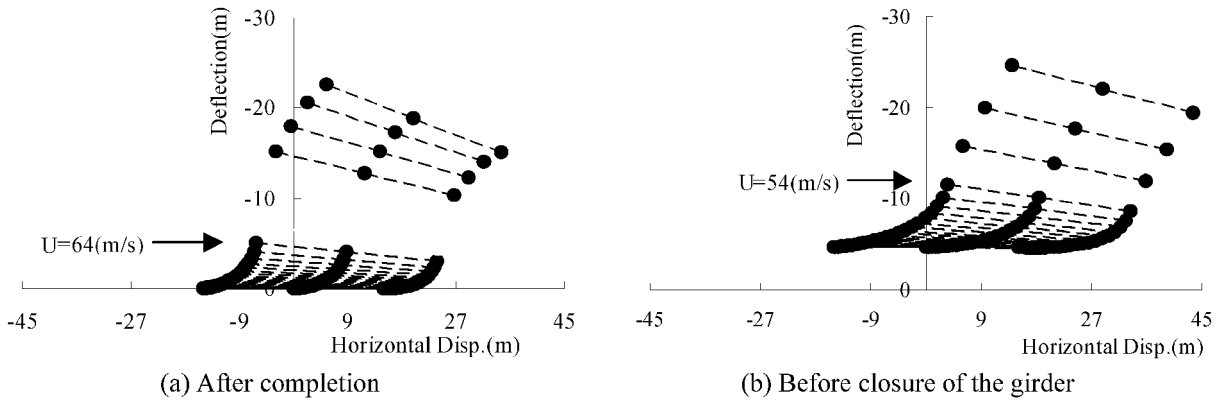

Figure 9. Track of the girder cross-section at center of the span (Used Type-I aerodynamic coefficients).

the material of the cable on out-of-plane instability under displacement-dependent wind load is investigated by using 3-D geometrical nonlinear analysis. The main results obtained from this study are summarized as follows.

(1)Instabilities of a completed bridge and a bridge under construction occur at the wind velocities of approximately 60 m/s and 50 m/s, respectively. They are smaller than flutter onset wind velocity.

(2)For the bridges both after completion and before connection of the girder, responses of the bridge using CFCC become smaller compared with those of the bridge using steel cable. In the case of this model with a span 1400-meters, around 10% reduction of the responses are obtained.

(3)In the bridge after completion, a jumping phenomenon occurs when angle of attack reaches 5 deg. This phenomenon does not occur in the bridge before connection of the girder, although the same aerodynamic coefficients are used.

Reference

[1] Shinichi Konno et al., "Material Properties of Carbon Fiber Cables for Cable Supported Bridges", *Bridge and Foundation Engineering,* pp. 29–32 (1990).

[2] Nonuaki Take et al., "Study on Aerodynamic Stability and Preliminary Design of Dual Cable Suspension Bridges using Advanced Composites", *Transactions of the Japan Society for Computational Engineering and Science, JSCES,* Vol. 1, pp. 89–94 (1999).

[3] Mei, K.-H. and Lu, Z.-T. "Application Prospect of CFRP to Super Length Suspension Bridge and Cable-Stayed Bridge", *Bridge Constructer, Mainland,* No. 2, pp.75–78 (2002).

[4] Kao, C.-S. et al, "Study on the Long-span Cable-stayed Bridges with Cable Fiber Composite Cables", *Asia Pacific Review of Engineering Science and Technology,* Vol. 3, pp. 297–318 (2005).

[5] Masatusgu Nagai et al., "Minimum Cross-Section Shape of Girder for Long Span Cable-Stayed Bridge Based on Static and Dynamic Instability Analysis", *Journal of Structural Mechanics and Earthquake Engineering, JSCE,* No. 633/I-49, pp. 155–167 (1999).

[6] Xie, X. et al., "Static Behaviors of Long-Span Cable-Stayed Bridge", *Journal of Structural Mechanics and Earthquake Engineering, JSCE,* No. 537/I-35, pp. 205–215 (1996).

[7] Kao, C.-S. and Kou, C.-H. "Study on Static Behavior and the Ultimate Load-Bearing Capacity of Long-span Cable-stayed Bridges", *Asia Pacific Review of Engineering Science and Technology,* Vol. 2, pp. 123–148 (2004).

[8] Kao, C.-S. et al, "Investigation on the Structural Behavior of Long-span Cable-stayed Bridges due to Cable Broken", *Asia Pacific Review Engineering Science and Technology,* Vol. 2, pp. 210–232 (2004).

[9] Xie, X. et al., "Nonlinear Analysis of Flexible Cable Based on Updated Lagrangian Formulation", *Journal of Structural Engineering, JSCE,* Vol. 41A, pp. 427–434 (1995).

[10] Hunter Rouse, "Elementary Mechanics of Fluids", John Wiley and Sons, Inc. New York (1946).

[11] Boonyapinyo, V., Yamada, H. and Miyata, T., "Nonlinear Buckling Instability Analysis of Long-Span Cable-Stayed Bridge under Displacement-Dependent Wind Load", *Journal of Structural Engineering, JSCE,* Vol. 39A, pp. 923–936 (1993).

Manuscript Received: May. 24, 2005
Accepted: Oct. 7, 2005

Call for Papers

Tamkang University was founded in 1950 and Tamkang Journal was published since 1962. Starting from 1998, Tamkang Journal was divided into two, which are Tamkang Journal of Science and Engineering and Tamkang Journal of Humanity and Social Science. Tamkang Journal of Science and Engineering became an international journal since 2000 and four issues are published each year. Tamkang Journal of Science and Engineering devotes to address the following broad research topics, including Computer Science of various aspects including software technologies, parallel/distributive computing, multimedia techniques and bio-informatics, Civil Engineering, Aerospace, Architecture Engineering, Mechanical Engineering, Electrical Engineering, Physics, Chemistry, Chemical Engineering, Biological Technology, Statistics and Environmental Science. Each issue will focus on a particular topic so that this journal can be the only journal that is persistently pursuing advanced researches from all areas. Each article published in this journal is included in COMPENDEX PLUS (EI). As such, we would like to sincerely invite you, the prestige and devoted researchers to submit your significant research results to Tamkang Journal of Science and Engineering. Your submission not only can significantly promote your research effort but also will superb our journal.